HOLOGIC®
The Science of Sure

Powerful images.
Clear answers.

Manage Patient's concerns about Atypical Femur Fracture*

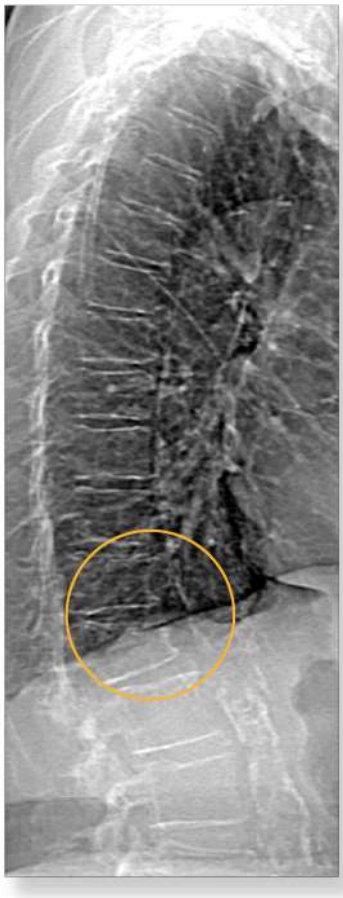

Vertebral Fracture Assessment – a critical part of a complete fracture risk assessment

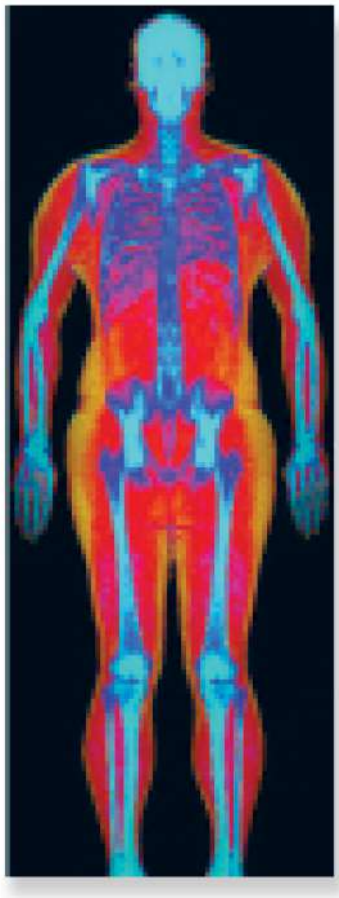

Advanced Body Composition® Assessment – the power to see what's inside

Contact your Hologic rep today at BSHSalesSupportUS@hologic.com

*Incomplete Atypical Femur Fractures imaged with a Hologic densitometer, courtesy of Prof. Cheung, University of Toronto

www.hologic.com | dxaperformance.com | 1.800.442.9892

ORIGINAL ARTICLE

JBMR®

RANKL Inhibition in Fibrous Dysplasia of Bone: A Preclinical Study in a Mouse Model of the Human Disease

Biagio Palmisano,[1] Emanuela Spica,[1] Cristina Remoli,[1] Rossella Labella,[1] Annamaria Di Filippo,[1] Samantha Donsante,[1] Fabiano Bini,[2] Domenico Raimondo,[1] Franco Marinozzi,[2] Alan Boyde,[3] Pamela Robey,[4] Alessandro Corsi,[1] and Mara Riminucci[1]

[1]Department of Molecular Medicine, Sapienza University, Rome, Italy
[2]Department of Mechanical and Aerospace Engineering, Sapienza University, Rome, Italy
[3]Dental Physical Sciences, Barts' and The London School of Medicine and Dentistry, Queen Mary University of London (QMUL), London, UK
[4]Skeletal Biology Section, National Institute of Dental and Craniofacial Research (NIDCR), National Institutes of Health (NIH), Bethesda, MD, USA

ABSTRACT

Fibrous dysplasia of bone/McCune-Albright syndrome (Polyostotic FD/MAS; OMIM#174800) is a crippling skeletal disease caused by gain-of-function mutations of $G_s\alpha$. Enhanced bone resorption is a recurrent histological feature of FD and a major cause of fragility of affected bones. Previous work suggests that increased bone resorption in FD is driven by RANKL and some studies have shown that the anti-RANKL monoclonal antibody, denosumab, reduces bone turnover and bone pain in FD patients. However, the effect of RANKL inhibition on the histopathology of FD and its impact on the natural history of the disease remain to be assessed. In this study, we treated the EF1α-$G_s\alpha^{R201C}$ mice, which develop an FD-like phenotype, with an anti-mouse RANKL monoclonal antibody. We found that the treatment induced marked radiographic and microscopic changes at affected skeletal sites in 2-month-old mice. The involved skeletal segments became sclerotic due to the deposition of new, highly mineralized bone within developing FD lesions and showed a higher mechanical resistance compared to affected segments from untreated transgenic mice. Similar changes were also detected in older mice with a full-blown skeletal phenotype. The administration of anti-mouse RANKL antibody arrested the growth of established lesions and, in young mice, prevented the appearance of new ones. However, after drug withdrawal, the newly formed bone was remodelled into FD tissue and the disease progression resumed in young mice. Taken together, our results show that the anti-RANKL antibody significantly affected the bone pathology and natural history of FD in the mouse. Pending further work on the prevention and management of relapse after treatment discontinuation, our preclinical study suggests that RANKL inhibition may be an effective therapeutic option for FD patients. © 2019 American Society for Bone and Mineral Research.

KEY WORDS: BONE REMODELLING; FIBROUS DYSPLASIA; DENOSUMAB; $G_s\alpha$; RANKL

Introduction

Fibrous dysplasia of bone/McCune-Albright syndrome (Polyostotic FD/MAS; OMIM#174800) is a genetic, non-inherited disease caused by gain-of-function mutations (mainly R201H and R201C) of the α subunit of the stimulatory G protein ($G_s\alpha$)[1,2] encoded by the *GNAS* gene (GNAS complex locus;GNAS, OMIM *139320). Consistent with the origin of the mutation in a pluripotent cell of the developing embryo,[3] mutated cells in postnatal life may be found in derivatives of all three embryonic germ layers. Thus, a wide range of tissues and organs (eg, skin, endocrine glands, skeletal muscles, bone) may be affected in variable combinations in FD/MAS patients. However, except for MAS cases with very early neonatal onset,[4] skeletal lesions usually represent the most severe, and less treatable, expression of the clinical phenotype because of bone pain, fracture, and deformity.[5]

The histopathology of FD typically features marrow fibrosis (fibroblast-like osteogenic precursors replacing adipocytes and haematopoiesis), abnormal bone trabeculae (with site-specific patterns of distribution), defective bone mineralization, and dysregulated osteoclast formation.[5–10] Overall, these changes convert normal bone and bone marrow into an architecturally disorganized and mechanically unsound fibro-osseous tissue. Increased osteoclastogenesis is thought to play a role in the establishment and progression of FD lesions and currently represents the only target for a medical therapy of the disease. Indeed, multiple studies have tested the effect of bisphosphonates (BPs) in FD patients, showing some clinical benefits (reduction of bone pain), but, in the absence of significant changes in the histology

Received in original form February 8, 2019; revised form June 13, 2019; accepted June 30, 2019. Accepted manuscript online July 11, 2019.
Address correspondence to: Mara Riminucci, MD, PhD, Department of Molecular Medicine, Sapienza University, Policlinico Umberto I, Viale Regina 324, 00161 Rome, Italy. E-mail: mara.riminucci@uniroma1.it
Additional Supporting Information may be found in the online version of this article.
Journal of Bone and Mineral Research, Vol. 34, No. 12, December 2019, pp 2171–2182.
DOI: 10.1002/jbmr.3828

and evolution of the skeletal phenotype.[11–15] Potential alternative approaches rely on the identification of the specific cellular and molecular mechanism(s) leading to the enhanced osteoclast formation within FD lesions. Increased expression of IL-6 has been previously identified as a molecular link between gain-of-function mutations of $G_s\alpha$ and enhanced osteoclastogenesis in FD.[10,16,17] Consequently, inhibition of IL-6 by has been considered as a potential treatment for the disease.[18]

Recently, a role for receptor activator of nuclear factor kappa-B ligand (RANKL; a member of the tumour necrosis factor superfamily and a potent stimulator of osteoclastogenesis[19,20]), in the disease has emerged from studies performed on human skeletal progenitors transduced with $G_s\alpha^{R201C}$,[21] transgenic mice expressing $G_s\alpha^{R201C}$ in skeletal cells,[22] and human FD tissue and cells.[23–25] In addition, serum levels of RANKL have been reported to be increased in mouse models that replicate human FD,[22,26] as well as in FD patients, in which they strongly correlated with the burden of the disease.[25] Accordingly, a limited number of studies have already tested the effect of the humanized anti-RANKL antibody, denosumab, in FD patients and have reported a positive effect on bone turnover, on the growth rate of lesions, as assessed by CT analysis, and on bone pain.[23,27–29] However, the role of RANKL in the histopathology of FD, as well as the effect of RANKL inhibition on the natural history of the disease, need to be investigated further.

We have previously generated transgenic mouse models with ubiquitous and constitutive expression of $G_s\alpha^{R201C}$ (EF1α-$G_s\alpha^{R201C}$ and PGK-$G_s\alpha^{R201C}$ mice)[30] that faithfully reproduce the essential pathological features of human FD and allow for controlled radiographic and histological studies in a sizable number of individuals. In this study, we tested the effect of RANKL inhibition on the skeletal phenotype of the EF1α-$G_s\alpha^{R201C}$ model. Following the assessment of RANKL expression in developing skeletal lesions, we have treated transgenic mice with an anti-mouse RANKL antibody and performed microradiographic, histologic, biochemical, and mechanical studies during the treatment and after its discontinuation. Overall, our results show that inhibition of RANKL profoundly affects the bone pathology and natural history of FD in the mouse, thus confirming that RANKL inhibition may be an effective therapeutic option for FD patients.

Materials and Methods

Mice and experimental groups

Generation and characterization of EF1α-$G_s\alpha^{R201C}$ mice were reported previously.[30] Briefly, the transgenic line was generated by lentiviral transgenesis using the constitutive promoter human elongation factor 1α (EF1α). In this mouse model, the mutant $G_s\alpha^{R201}$ sequence is germline transmitted and the genetic mosaicism typical of human FD is not reproduced. However, similarly to the human disease, FD-like lesions appear in the postnatal life and develop according to an asymmetric and metachronous temporospatial pattern. The animals were maintained in cabin-type isolators at standard environmental conditions (temperature 22°C to 25°C, humidity 40% to 70%) with 12:12 dark/light photoperiod. Food and water were provided ad libitum.

All studies were performed in compliance with relevant Italian laws and Institutional guidelines and all procedures were IACUC approved. Transgenic mice were selected based on radiographically detectable FD-like lesions in the tail vertebrae and femurs and were treated with an anti-mouse RANKL monoclonal antibody (mAb; Clone IK22/5; Bio X Cell, West Lebanon, NH, USA). Twenty-four EF1α-$G_s\alpha^{R201C}$ young mice (22 females and two males, 2 months of age) with developing FD-like skeletal lesions and four EF1α-$G_s\alpha^{R201C}$ adult mice (two females, 8 months old; one female and one male, 12 months old) with extensive, full-blown FD-like lesions were treated with 300 μg/mouse of either anti-RANKL mAb[31] or rat IgG2a isotype control (clone 2A3; Bio X Cell, West Lebanon, NH, USA) by intraperitoneal injection, twice a week for 14 weeks.

In the 2-month-old group, one-half of the mice were euthanized at the end of treatment (anti-RANKL group $n = 6$; isotype control group $n = 6$) and the other one-half underwent a 12-week follow-up (anti-RANKL group $n = 6$; isotype control group $n = 6$). Radiographic analysis was performed at different time points when serum samples were also collected for the evaluation of biochemical markers of bone turnover. During all of the experiments, mice were carefully monitored and no important adverse events were observed. In addition, to test the effect of anti-RANKL administration and cessation in the absence of any $G_s\alpha^{R201C}$-dependent change, such as endocrine abnormalities, which could potentially affect the result, four FVB/NJ wild-type mice (WT) (Jackson Laboratories,

Table 1. Experimental Groups

Group	Age	Treatment	Follow-up	*n*
EF1α-Gsα^{R201C}	2 months	Anti-RANKL mAb	–	6
			+	6
		Rat IgG2a isotype control	–	6
			+	6
	12 months	Anti-RANKL mAb	–	2
		Rat IgG2a isotype control	–	2
FVB/NJ (WT)	2 months	Anti-RANKL mAb	–	2
			+	2

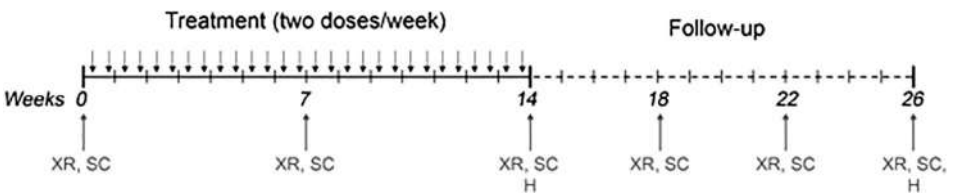

Fig. 1. Study design schema. H = histology; SC = serum collection; XR = radiographs.

Bar Harbour, ME, USA) were treated at 2 months of age according to the same regimen used for transgenic mice. Two mice were euthanized after 14 weeks of treatment and two mice after 14 weeks of treatment plus 12 weeks of follow-up.

The study design schema and the experimental groups are summarized in Fig. 1 and in Table 1, respectively.

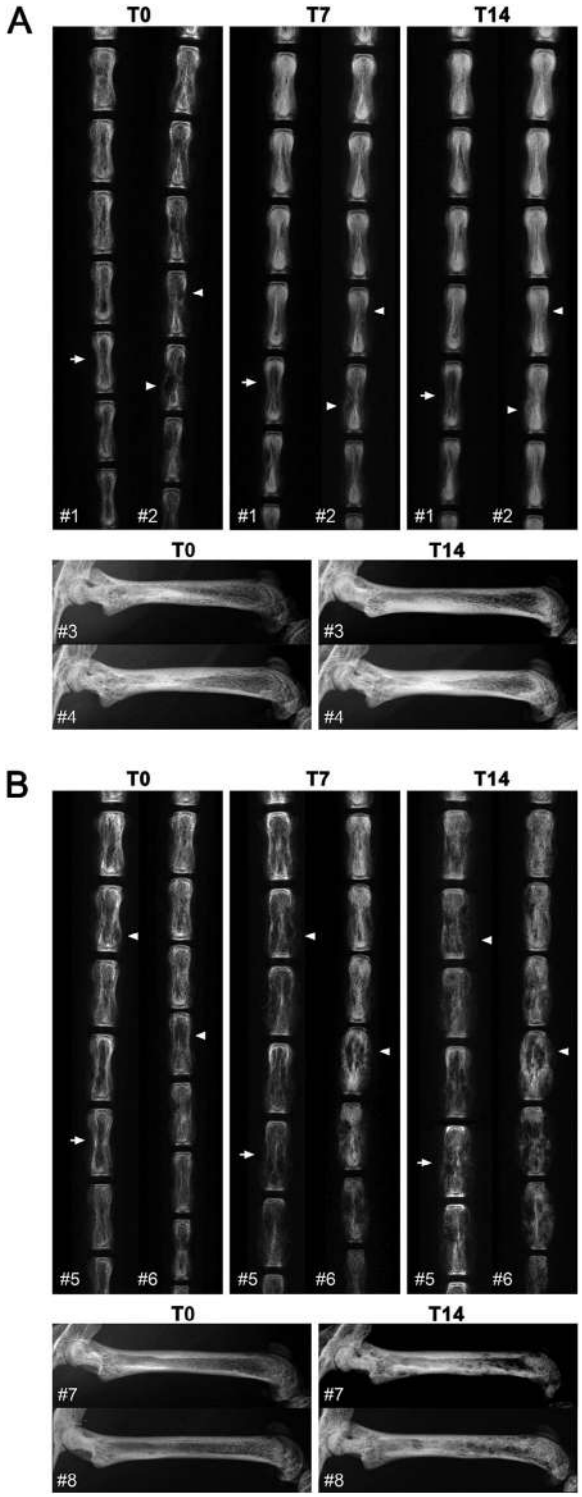

Additional methods (microradiography, biochemical markers, histology, histomorphometry, backscattered scanning electron imaging–scanning electron microscopy [BSE-SEM], RANKL immunolocalization, biomechanical analysis, and statistics) are reported in the Supporting Materials and Methods.

Results

RANKL inhibition reverted osteolysis and prevented progression of the radiographic FD-like phenotype in EF1α-$G_s\alpha^{R201C}$ mice

The expression of RANKL in the FD-like tissue of EF1α-$G_s\alpha^{R201C}$ mice was confirmed by immunohistochemistry (Supporting Fig. SS1). Twenty-four transgenic mice at 2 months of age were selected based on the radiographic phenotype, randomly assigned to the anti-RANKL (n = 12) or isotype control (n = 12) group and treated for 14 weeks. All mice showed irregular endosteal/medullary profiles and cortical lytic areas in the tail vertebrae (Fig. 2, T0) consistent with FD lesions at early/intermediate stage of development. Early endosteal changes were also present in four femurs in the anti-RANKL group and in five femurs in the isotype control group (Fig. 2, T0).

In mice receiving the anti-RANKL mAb, cortical lytic areas in the tail vertebrae were no longer detectable at the first radiographic survey performed after 7 weeks of drug administration (Fig. 2*A*, T7). At this time, the radiodensity of the tail vertebrae was higher compared to the pretreatment stage and, in some segments, further increased during the following 7 weeks of drug administration (Fig. 2*A*, T14). However, at all time points during the treatment, the radiographic aspect of the individual vertebrae was variable and apparently dependent on the initial burden of the disease. Segments with large osteolytic lesions and prominent irregularity of the endosteal profile at T0 showed a sclerotic appearance with narrowing/obliteration of the medullary cavity (Fig. 2*A*). On the other side, slightly affected or apparently unaffected vertebrae maintained their normal shape with no significant change in the profile and transparency of the medullary canal (Fig. 2*A*). Neither new osteolytic lesions nor bone deformities were detected during or at the end of the treatment.

Fig. 2. Skeletal radiographic changes during treatment with either anti-RANKL mAb (*A*) or rat IgG2a isotype (*B*) in young EF1α-$G_s\alpha^{R201C}$ mice. (*A*) Serial Faxitron analysis of two representative tails and femurs at different time points during the treatment with anti-RANKL mAb. In the tails (mice #1 and #2, upper panel), bone density increased in all the affected vertebrae, with progressive disappearance of the intracortical lytic lesions (arrowheads). In slightly affected or apparently unaffected segments (arrows), the vertebral shape and the profile and transparency of the medullary canal were maintained. In the femurs (mice #3 and #4, lower panel), in which very early lesions were recognized as thickening of the cortex at midshaft (T0), no progression of the disease was observed (T14). (*B*) Serial Faxitron analysis of two representative tails (mice #5 and #6, upper panel) and two femurs (mice #7 and #8, lower panel) at different time points during the treatment with rat IgG2a isotype. The disease evolved in all the affected vertebrae (arrowheads) and appeared in unaffected vertebrae (arrows) with progressive deformity and lytic changes. In the femurs, the lesions expanded progressively and at T14 almost the whole skeletal segment was involved with a combined lytic and sclerotic phenotype.

In contrast, in control mice, the radiographic phenotype steadily progressed with enlargement of preexistent areas of cortical radiolucency and appearance of new lytic foci and bone deformities, also in vertebrae that were not affected at T0 (Fig. 2*B*). Similar findings were observed in the affected femurs (Fig. 2*A*, *B*). Importantly, radiographic analysis of all femoral segments clearly showed that RANKL inhibition also prevented the progression of the phenotype across the skeleton (Supporting Fig. SS2). None of the 20 unaffected femurs of the anti-RANKL–treated mice developed radiographically detectable lesions during the treatment (Supporting Fig. SS2A). In contrast, at T14, a radiographically detectable phenotype appeared in 11 of 19 femurs that were normal at T0 in the isotype control group (Supporting Fig. SS2A), in agreement with the emergence of femoral lesions between 2 and 5 months of age in the EF1α-$G_s\alpha^{R201C}$ mouse strain.[30] To assess whether RANKL inhibition could also modify the radiographic phenotype in fully developed (final stage) murine FD, we then treated two adult EF1α-$G_s\alpha^{R201C}$ mice bearing lytic-sclerotic (ground-glass) FD-like lesions. After 14 weeks of treatment, a homogeneous opacity of the tail vertebrae and femurs was observed in both animals receiving the anti-RANKL mAb (Fig. 3*A*), while the radiographic phenotype became more severe in control mice (Fig. 3*B*).

RANKL inhibition led to deposition of highly mineralized bone within FD-like lesions of EF1α-$G_s\alpha^{R201C}$ mice

After 14 weeks of treatment, we euthanized six anti-RANKL-mAb mice and six rat IgG2a isotype mice that started the treatment at 2 to 3 months of age, and all of the adult mice. Consistent with the radiographic results, histology of the tail vertebrae showed that RANKL inhibition led to deposition of newly formed bone within the lesions. In young mice (Fig. 4), the amount of bone tissue clearly varied in the different segments according to the radiographic phenotype at the beginning of the anti-RANKL mAb administration. Bone deposition was extensive in vertebrae with pronounced lesions and led to the virtual obliteration of the medullary cavity (Fig. 4*A*,*E*,*G*). In contrast, no evidence of intramedullary bone formation was observed in tail vertebrae that were radiographically free of the disease at T0 (Fig. 4*C*) or in other unaffected skeletal segments. FD-like changes were observed in all of mice that received rat IgG2a isotype (Fig. 4*B*,*D*,*F*,*H*). Furthermore, a thorough histological analysis of multiple radiographically normal skeletal segments from both experimental groups confirmed the absence of lesions in the anti-RANKL mAb–treated mice, but revealed the presence of microscopic foci of disease in bones from the isotype control group (Supporting Fig. SS2B). Analysis of von Kossa/methylene blue–stained sections and BSE-SEM images showed the absence of excess osteoid in the newly formed bone (Fig. 5*A*,*C*,*E*) in contrast with samples from rat IgG2a isotype–treated mice (Fig. 5*B*,*D*,*F*). In addition, quantitative BSE (qBSE) showed a higher mineral content in the newly formed bone compared to both FD-bone and unaffected cortical bone (Fig. 5*G*,*H*). Consistent with the histological changes, the mechanical properties of anti-RANKL mAb–treated tail vertebrae improved. Compressive tests analysis revealed that the maximum load and axial stiffness of the specimens from treated mice were significantly increased compared to control samples (Fig. 6*A*,*B*). Neither multinucleated osteoclasts nor mononucleated osteoclast progenitors were recognized by morphology, TRAP histochemistry, or iodine-stained BSE-SEM image analysis in RANKL-inhibited mice (Supporting Fig. SS3A,C), whereas they

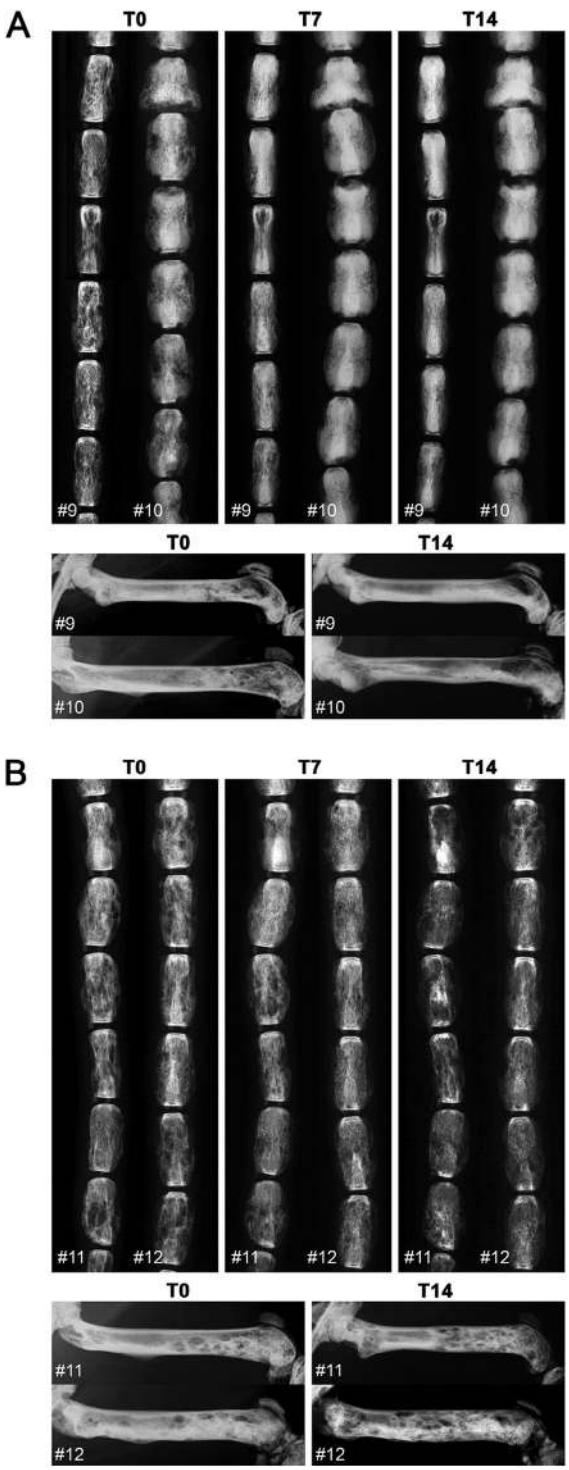

Fig. 3. Skeletal radiographic changes during treatment with either anti-RANKL mAb (*A*) or rat IgG2a isotype (*B*) in adult EF1α-$G_s\alpha^{R201C}$ mice. (*A*) Serial Faxitron analysis of two mice (mice #9 and #10) treated with the anti-RANKL mAb showing tail vertebrae (upper panel) and femurs (lower panel). At T0 all bones bore FD-like lesions with a ground-glass appearance, and, as in young mice, the treatment progressively enhanced their radiographic density (T14). (*B*) Serial Faxitron analysis of two adult mice (mice #11 and #12) treated with rat IgG2a isotype at the same time points showing tail vertebrae (upper panel) and femurs (lower panel). The lesions progressed leading to deformities of the skeletal segments.

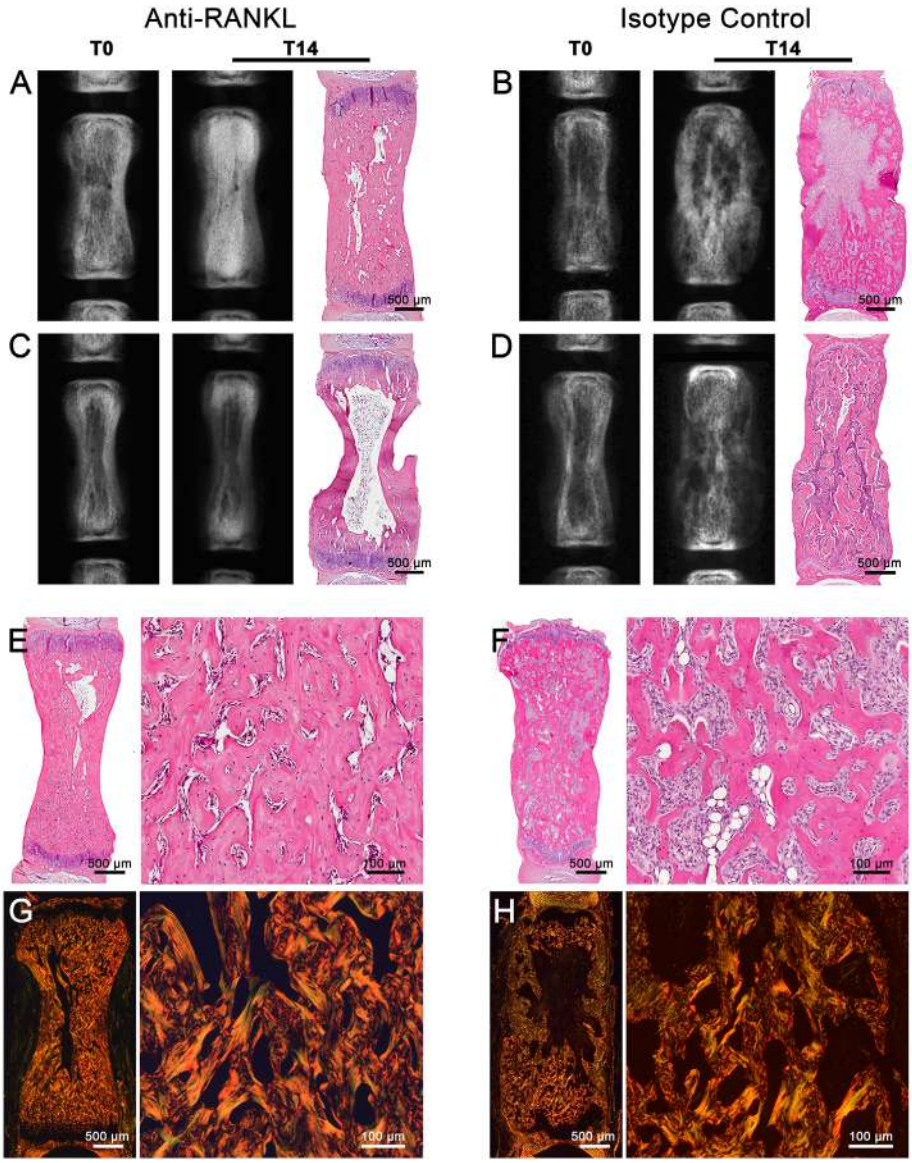

Fig. 4. (*A–D*) Correlation between radiographic and histological changes in young EF1α-$G_s\alpha^{R201C}$ mice. H&E-stained histological sections of tail vertebrae that were radiographically affected at T0 revealed newly deposited bone after anti-RANKL mAb treatment (*A*) and FD-like fibro-osseous tissue after rat IgG2a isotype treatment (*B*). Tail vertebrae that were radiographically free of disease at T0 showed a normal morphology after anti-RANKL mAb treatment (*C*) and an FD-like appearance after rat IgG2 isotype administration (*D*). Replacement of the FD-like fibro-osseous tissue by newly formed bone occurred in the anti-RANKL mAb–treated mice (*E*: H&E, transmitted light; *G*: Sirius red, polarized light), but not in mice receiving the rat IgG2a isotype (*F*: H&E, transmitted light; *H*: Sirius red, polarized light).

were numerous and irregularly distributed within the fibrosis and on the bone surfaces in control mice (Supporting Fig. SS3B,D). In addition, in mice treated with the anti-RANKL mAb, inhibition of osteoclastogenesis prevented the resorption of the metaphyseal mineralized cartilage at the growth plates. As a consequence, metaphyses appeared radiographically sclerotic (Supporting Fig. SS4A,B) and showed persistence of cartilaginous cores reflecting the failure of transition from primary to secondary spongiosa (Supporting Fig. SS4C,D,E). Increased density at the metaphyseal regions was the only radiographically detectable change induced by RANKL inhibition in WT mice (data not shown). Extensive bone deposition was also observed during anti-RANKL mAb treatment in adult mice with full-blown FD-like phenotype (Supporting Fig. SS5). However, in these mice, at variance with young animals, small areas of fibrotic tissue persisted among the newly formed bone. Histomorphometry showed that in young mice the mean amount of total bone was significantly higher in the anti-RANKL mAb group compared to controls (Fig. 6*C*), due to the replacement of the preexisting FD tissue by newly formed bone. The mean amount of adipose marrow was also significantly higher compared to controls, indicating that marrow adipocytes were not replaced by the FD tissue during the anti-RANKL mAb treatment. In the tail vertebrae of adult mice treated with the anti-RANKL mAb (Fig. 6*D*), the increase in the total amount of bone was even more evident because of the greater extent of the

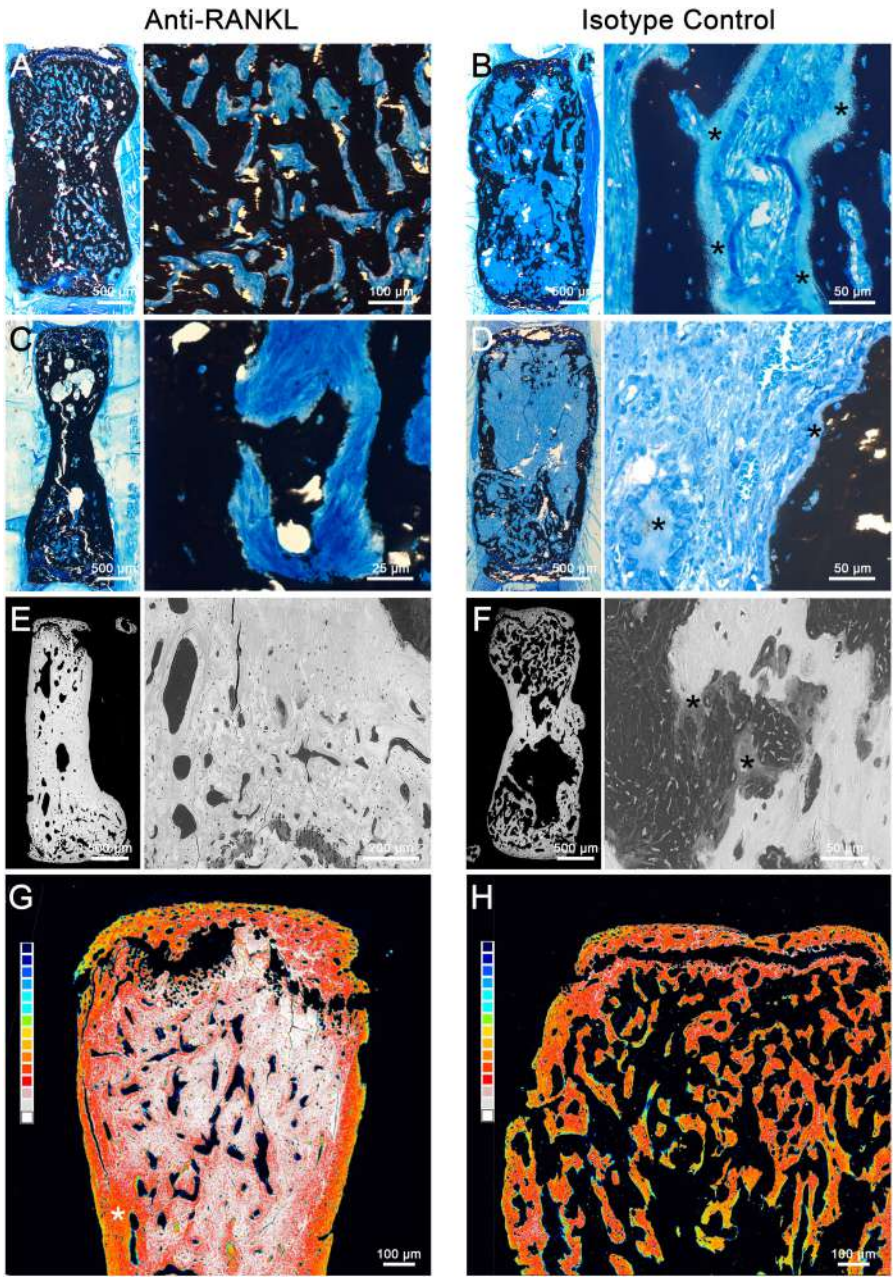

Fig. 5. Von Kossa/methylene blue–stained sections of nondecalcified bone samples showed extensive mineralization of the bone matrix in tail vertebrae from young anti-RANKL mAb–treated mice (*A*, *C*) and excess of osteoid (ie, unmineralized bone matrix) in tail vertebrae from rat IgG2a isotype–treated mice (*B*, *D*). The same findings were observed in BSE-SEM images of tail vertebrae from anti-RANKL mAb–treated (*E*) and rat IgG2a isotype–treated (*F*) mice. qBSE analysis revealed a higher level of mineralization of the newly formed bone in the tail vertebrae of anti-RANKL mAb–treated mice (*G*) compared with cortical unaffected bone (*G*) and FD bone of tail vertebrae from rat IgG2a isotype–treated mice (*H*). Black asterisks in *B*, *D*, and *F*: Osteoid. White asterisk in *G*: Cortical unaffected bone. qBSE = quantitative BSE.

lesional tissue at the beginning of the treatment, although the fibrotic marrow was not entirely replaced by bone.

Recurrence of the radiographic and histological FD-like phenotype in EF1α-$G_s\alpha^{R201C}$ mice during the follow-up

To assess whether, and how long, the radiographic and microscopic changes induced by RANKL inhibition persisted after the withdrawal of the antibody, we carried out a follow-up study on some mice that started the treatment at 2 months of age. Mice were radiographically monitored for 12 weeks (Fig. 7, T18–T26). The first Faxitron analysis performed after 4 weeks from the last injection of the drug showed a reduction in the radiodensity and the appearance of small lytic areas in some tail vertebrae (Fig. 7*A*, T18). At the end of the follow-up, radiographically evident lesions were detected in the tails (Fig. 7*A*, T26) and in other skeletal segments (data not shown) and the phenotype was overall comparable to that of control mice (Fig. 7*B*, T26).

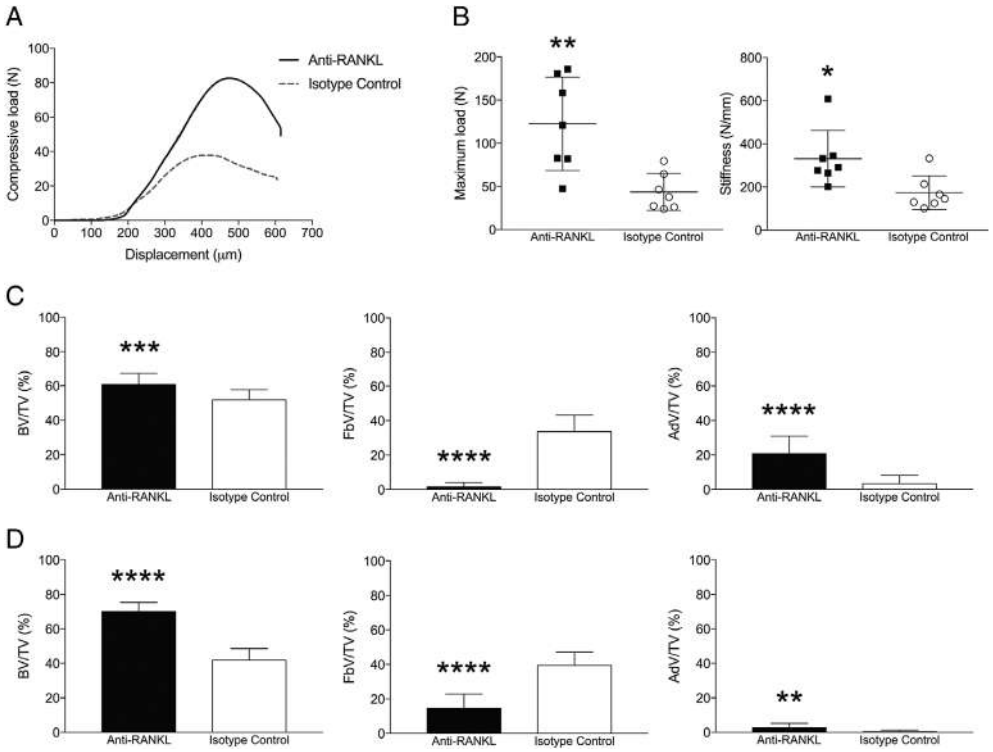

Fig. 6. (*A*, *B*) Biomechanical analysis of the tail vertebrae. (*A*) Two representative load–displacement curves generated from vertebral compression test performed on one tail vertebra from an anti-RANKL mAb–treated mouse and one tail vertebra from a rat IgG2a isotype–treated mouse. (*B*) The comparative analysis of maximum load and stiffness, computed from the load–displacement curves, reveals an increase of 180% and 90% respectively in anti-RANKL mAb–treated compared to rat IgG2a isotype–treated mice. (*C*, *D*) Histomorphometric analysis of volumes of bone (BV/TV), fibrous (FbV/TV), and adipose (bone marrow AdV/TV) tissues performed on histological sections obtained from the tail vertebrae at the end of the treatment with either anti-RANKL mAb or rat IgG2a isotype in young (*C*) and adult (*D*) mice. In both groups, the mean amount of BV/TV and AdV/TV was significantly higher and that of FbV/TV significantly lower in anti-RANKL mAb–treated mice compared to the rat IgG2a isotype–treated groups. *$p < 0.05$; **$p < 0.01$; ***$p < 0.001$; ****$p < 0.0001$. AdV/TV = adipose tissue volume/total volume; BV/TV = bone volume/total volume; FbV/TV = fibrous tissue volume/total volume.

Accordingly, a fibro-osseous tissue including abnormal and osteomalacic trabeculae and multiple osteoclasts was observed by microscopic analysis (Fig. 8*A-H*). In WT mice, following anti-RANKL withdrawal, a reduction of the metaphyseal density compared to T14 was observed at the end of follow-up (data not shown).

Biochemical profile of EF1α-$G_s\alpha^{R201C}$ mice during and after RANKL-inhibition

Serum samples from young mice were harvested before (T0), during (T7), and at the end (T14) of the treatment, and once a month (T18, T22, and T26) during the follow-up. Serum total calcium levels (Fig. 9*A*) remained similar in the anti-RANKL mAb and control group during the treatment. As expected, they significantly increased in mice that received the anti-RANKL mAb shortly after the discontinuation of the drug. However, at the end of the follow-up no statistically significant difference was observed between the two cohorts of animals. Serum phosphate levels (Fig. 9*B*) remained comparable in the two groups throughout the treatment and during follow-up. CTX-1 levels (Fig. 9*C*) significantly decreased at week 7 and 14 in the anti-RANKL group and significantly increased shortly after drug withdrawal (T14 versus T18, $p = .0029$). Serum levels of P1NP (Fig. 9*D*) were significantly reduced during the anti-RANKL mAb treatment compared to controls and significantly increased during the follow-up (T14 versus T22, $p = .0220$). Serum levels of both markers returned to the initial values (T0) at the end of the follow-up.

Discussion

The genetic nature of FD calls for the development of therapies based on transplantation of normal skeletal stem cells (keeping in mind the somatic mosaic nature of the disease) and/or genetic correction as the only possibility to eradicate the disease.[3] These approaches are feasible in principle and have also been shown to be effective in appropriate experimental systems.[21] However, translational studies are impeded by the complex structure and physiology of the skeleton, in addition to the gain-of-function effect of the $G_s\alpha$ mutation. Besides corrective surgery, alternative, although not radical, modalities of intervention rely on approaches able to target the key morbidity factors of the disease. Recently, attention has been focused on denosumab,[32] a US Food and Drug Administration (FDA)-approved therapeutic option for osteoporosis and skeletal

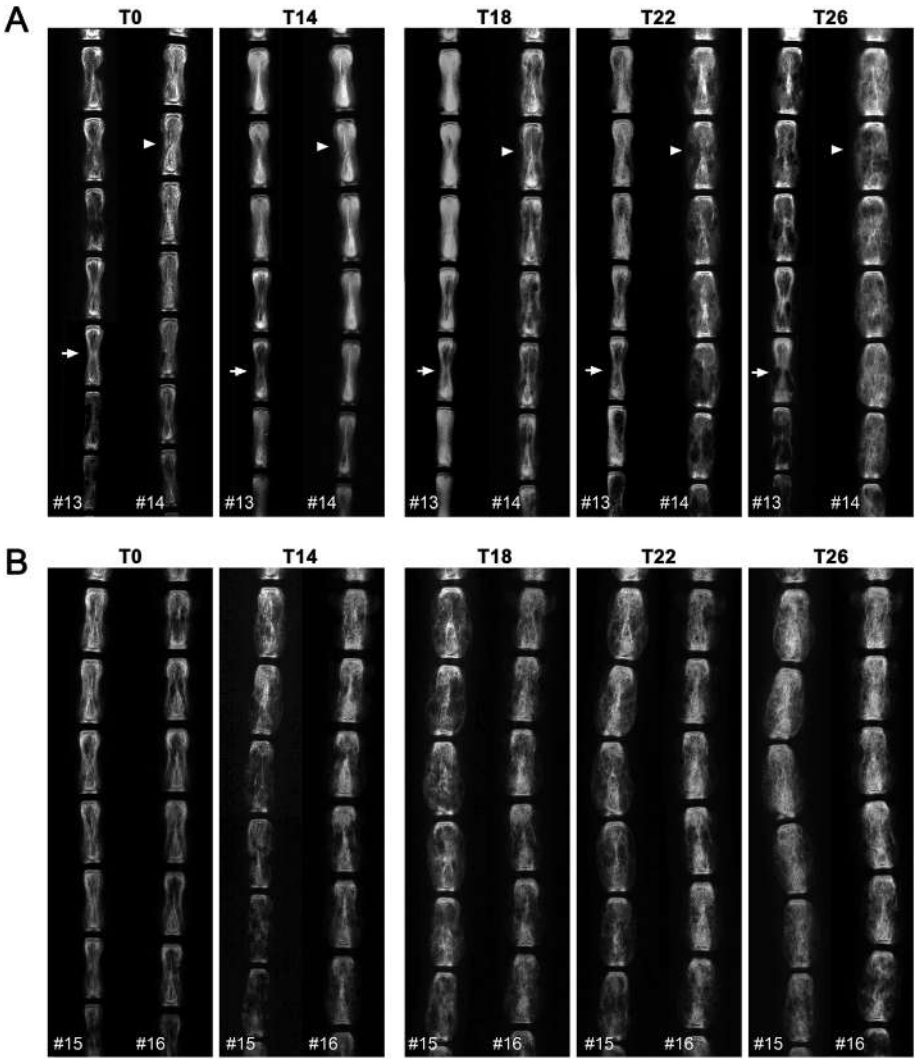

Fig. 7. Radiographic changes during the 12-week follow-up in the tail vertebrae of EF1α-$G_s\alpha^{R201C}$ mice treated for 14 weeks with either anti-RANKL mAb (*A*, mice #13 and #14) or rat IgG2a isotype (*B*, mice #15 and #16). Reduced bone density and osteolytic areas were detected in some anti-RANKL mAb–treated mice at the first radiographic analysis performed after drug discontinuation (T18, mouse #14). At the end of the follow-up (T26), radiographs of the tail vertebrae of mice treated with the anti-RANKL mAb showed recurrence of original lesions (arrowheads) and completely new lesions in vertebrae that were radiographically unaffected at the beginning of the treatment (arrows).

conditions featuring increased osteoclast activity, such as giant cell tumour of bone, and cancer metastasis.[33–37]

To clarify the effect of RANKL-inhibition on the radiographic and histological expression of FD, we took advantage of our transgenic murine model of the disease[30] that allowed us to investigate the effects of an anti-mouse RANKL-mAb in a sizable number of individuals, homogenous for age and type of lesion. The use of our model was further validated by the demonstration that, as in FD patients,[23–25] in EF1α-$G_s\alpha^{R201C}$ mice the fibrodysplastic tissue was a source of RANKL. In addition, as in primates and humans under treatment with denosumab,[35–38] a sustained decrease of both CTX-1 and P1NP occurred during the administration of the anti-RANKL mAb.

Our data show that RANKL inhibition in EF1α-$G_s\alpha^{R201C}$ mice led to the deposition of highly mineralized bone at affected skeletal sites. In contrast, changes in nonaffected bones were similar to those observed in WT mice and consisted in sclerotic metaphyseal bands that resulted from the failure of transition from primary to secondary spongiosa and reduced after cessation of the anti-RANKL mAb administration. According to our preliminary data, these physeal cartilage changes did not interfere with the growth of the skeletal segments (data not shown). However, further in-depth studies are required to better assess this point, which represents a very important question in children with FD.

The replacement of the FD tissue with mineralized bone implies that the treatment reverted the two major tissue changes that underlie the bone fragility and the clinical morbidity of the disease; ie, osteolysis and osteomalacia. It must be noted that the radiographic and/or histological changes observed with the anti-RANKL mAb have never been reported following treatment of FD lesions with BPs,[11–13] which inhibit the activity but not the formation of osteoclasts. The different effect of the two types of antiresorptive agents strongly suggests that osteoclasts and/or osteoclast

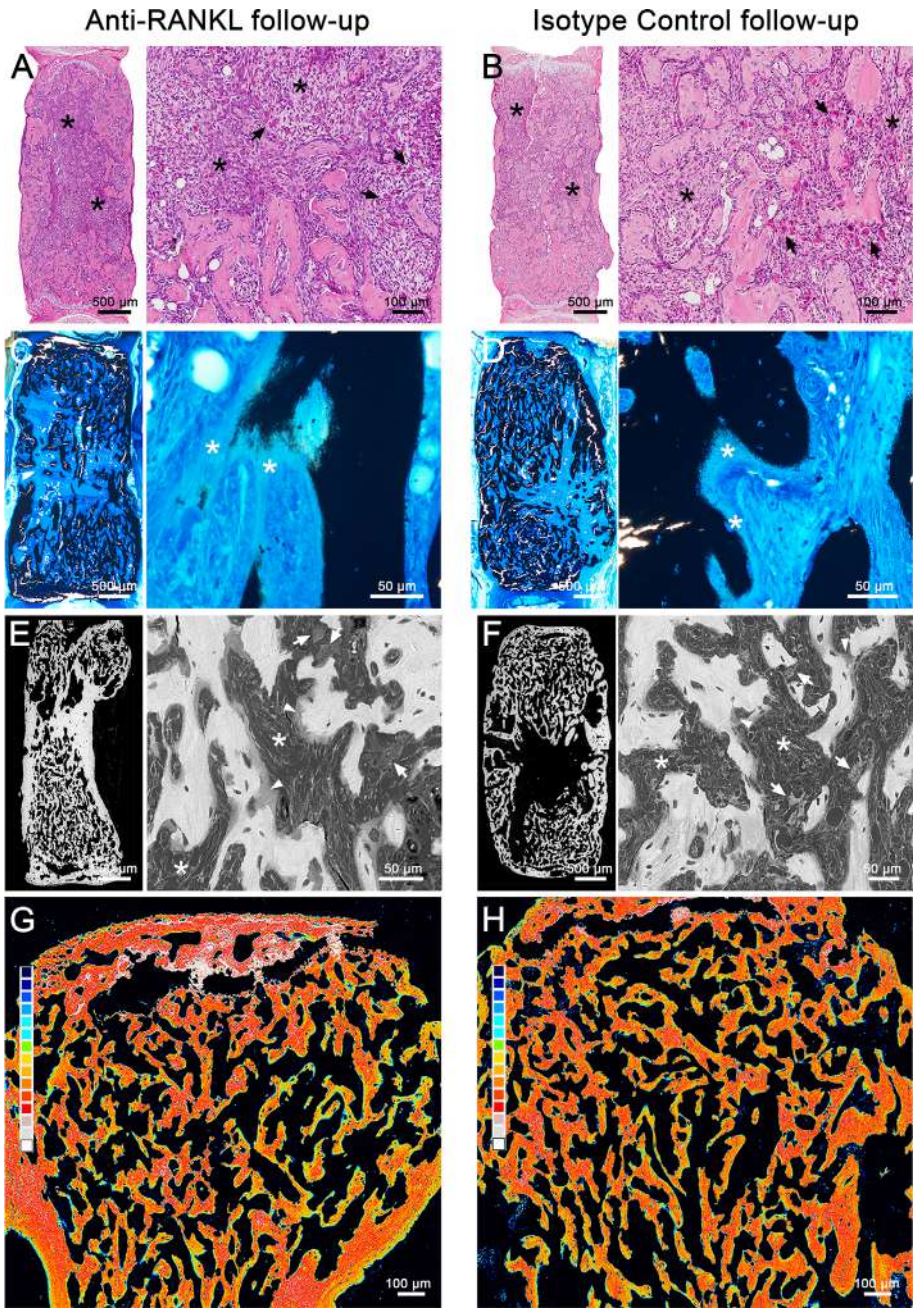

Fig. 8. Histology of tail vertebrae of mice euthanized at the end of the 12-week follow-up (T26). In H&E-stained sections of anti-RANKL–treated mice (*A*) the amount of osteoclasts (arrows) and fibrous tissue (asterisks) was comparable to that observed in rat IgG2a isotype–treated animals (*B*). Undecalcified, Von Kossa/methylene blue–stained sections showed numerous tiny bone trabeculae with a thick layer of osteoid in both anti-RANKL mAb–treated (*C*, asterisks) and rat IgG2a isotype–treated (*D*, asterisks) mice. BSE-SEM images of vertebrae from mice treated with anti-RANKL mAb (*E*) and rat IgG2a isotype (*F*) showed fibrous marrow (asterisks), osteoclasts (arrows), and intralesional undermineralized bone trabeculae (arrowheads). qBSE revealed a similar content of mineral in the bone matrix of the lesional bone in anti-RANKL–treated (*G*) and rat IgG2a isotype–treated (*H*) mice. qBSE = quantitative BSE.

precursors, independent on their resorption activity, negatively modulate osteogenic differentiation within the FD tissue and the deposition of mineralized bone. If the recently reported secretion of molecular factors and extracellular vesicles by osteoclasts[39,40] is involved in the effect of RANKL inhibition in FD must be investigated in future studies. Interestingly, Ohishi and colleagues[41] previously compared the effect of osteoprotegerin (OPG) and BPs in a mouse model of constitutive activation of the PTH/PTHrP receptor that transiently reproduces histological features of FD.[42] They reported that OPG (which reduced osteoclast activity and number), but not BPs (which reduced only osteoclast activity), abrogated marrow fibrosis in their mouse model and suggested that the differential effect could be dependent on the reduced number of osteoclasts in OPG-treated mice.

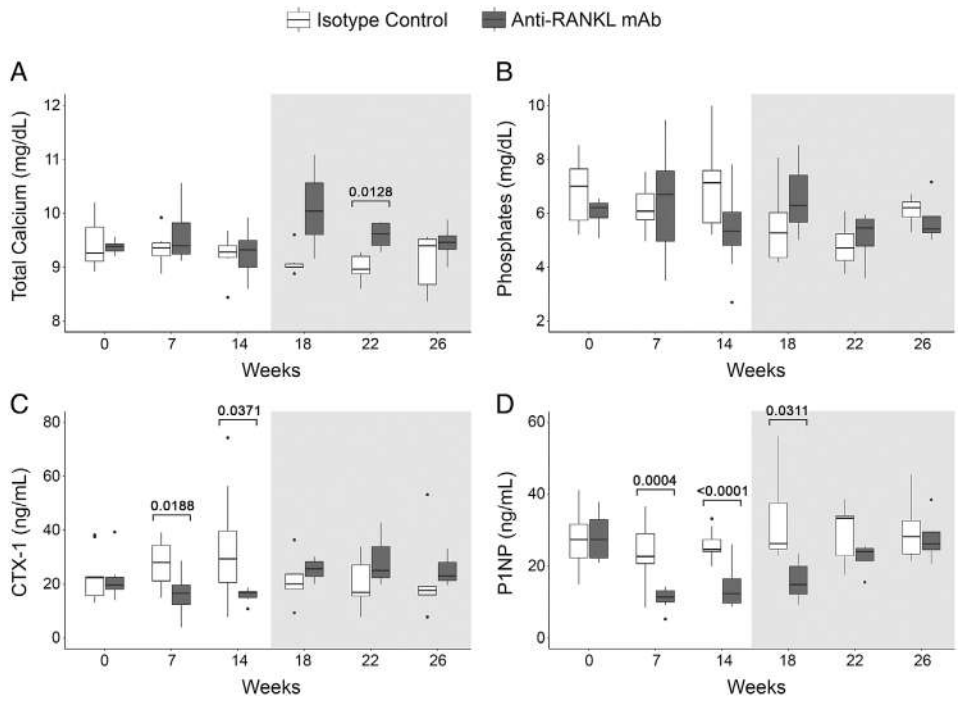

Fig. 9. Serum analysis performed during the treatment and follow-up in anti-RANKL mAb–treated mice and in rat IgG2a isotype–treated mice. Box plots show the serum levels of total calcium (*A*), phosphate (*B*), CTX-1 (*C*), and P1NP (*D*) at different time points. Outliers are represented as single spots outside the limits of the box. The significant *p* values from *t* test comparison of anti-RANKL mAb versus rat IgG2a isotype mice at specific time points are reported. The grey field in all graphs shows the follow-up period. During treatment, serum calcium (*A*) and phosphate (*B*) levels did not show significant changes. In contrast, CTX1 (*C*) and P1NP (*D*) were significantly reduced in the anti-RANKL group. In the follow-up period, a statistically significant difference was observed for total calcium and P1NP serum levels at 22 and 18 weeks, respectively. Moreover, comparative analysis between the mean values for all the measured parameters at the end of the treatment (T14) and at the different time points during the follow-up in the anti-RANKL group showed an increase, even though not significant, for calcium and phosphate at T18 and a significant increase for CTX at T18 ($p = 0.0029$) and for P1NP at T22 ($p = 0.0220$). At the end of follow-up, serum levels for all the measured parameters were not significantly different between anti-RANKL mAb–treated and rat IgG2a isotype–treated mice.

Another interesting finding of our work was the increased mineral content of the newly formed bone compared to the untreated FD bone and also to cortical unaffected bone, as established by qBSE analysis. This result could be directly dependent on the inhibition of remodeling within the FD tissue. As reported[43] in high bone-remodeling conditions, bone multicellular units (BMUs) do not reach the maximum levels of mineralization because their lifespan is reduced by the continuous appearance of new BMUs. Accordingly, the reduction in the remodeling rate associated with the antiresorptive drugs might favour the mineralization of the extracellular matrix by allowing a higher number of BMUs to reach their maximal mineralization capacity.[38] It is possible that in our mouse model, inhibition of bone resorption resulted in the saturation of calcium hydroxyapatite in preexisting undermineralized bone matrix as well as in the osteoid that was rapidly deposited during the treatment with the anti-RANKL mAb.[44] Even though we cannot exclude the occurrence of a dystrophic calcification rather than a physiological mineralization process (because we did not compare the structure and mechanical properties of the newly formed bone to those of WT mouse bone), the deposition of a highly mineralized bone in anti-RANKL–treated mice translated into a significant improvement in the biomechanical properties (namely maximum load and axial stiffness) of the FD-affected skeletal segments compared with those obtained from rat IgG2a isotype–treated mice.

Our data also show that treatment of older mice with an advanced bone phenotype with anti-RANKL mAb did not completely reproduced the effect observed in young mice with recent lesions. Although this result could be potentially ascribed to an insufficient drug dosage in old mice with full-blown disease, it may also suggest that in longstanding FD lesions, the $G_s\alpha$ mutated, and perhaps the genetically normal, osteogenic cells have a reduced ability to complete osteoblastic differentiation per se, due to the abnormal microenvironment and/or aging. This would imply that the anti-RANKL treatment should be started as early as possible in FD in order to achieve the best results, not only for prevention but also for reversion of the disease. Finally, as expected, the withdrawal of the anti-RANKL antibody in FD mice was associated with the resumption of osteoclast formation and bone resorption. This was associated with the recurrence of skeletal lesions for which the impact of the germline mutation in our mouse model (compared to the somatic mosaicism observed in humans) remains to be assessed.

In conclusion, our data show that RANKL inhibition in mice reproducing human FD had a relevant effect on the radiographic and histological appearance of the skeletal phenotype and suggest that denosumab may be a treatment option for the human

disease, even though the disease relapse observed with discontinuation of treatment remains problematic. In addition, further studies are required to test in mice dosing regimens comparable to those currently used in human diseases. In our study, the anti-RANKL mAb dosing used was estimated[45,46] to be lower compared to the 12-month course of denosumab that was planned in Boyce and colleagues,[23] and, to a greater extent, to those currently used in human diseases such as giant cell tumour of bone.[47] Our work also suggests that osteoclasts may be involved in the pathogenesis of FD through mechanisms not necessarily related to bone resorption. Unveiling these molecular mechanisms could lead to a better understanding of the pathogenesis of the disease and to the identification of new specific therapeutic targets.

Disclosures

All authors state that they have no conflicts of interest.

Acknowledgments

This study was supported by grants from Telethon (GGP15198) to MR; University of Pennsylvania Orphan Disease Center in partnership with the Fibrous Dysplasia Foundation MDBR17-114-FD/MAS to MR and MDBR-18-114-FD/MAS to MR and AC; and Sapienza University to AC. We thank Prof. Paolo Bianco (1955–2015) for his fundamental contribution to the understanding of fibrous dysplasia/McCune-Albright syndrome.

Authors' Roles: Study design: AC, BP, PR, and MR. Radiographic and histological studies: BP, ES, CR, RL, ADF, and SD. Mechanical tests: FB and FM. BSE-SEM analysis: AB. Statistical analysis: DR. Drafting manuscript: BP, AC, and MR. Revising manuscript: AB, PR, AC, and MR. Approving the final version of the manuscript: BP, ES, CR, RL, ADF, SD, FB, DR, FM, AB, PR, AC, and MR. BP, AC, and MR take responsibility for the integrity of the presented data.

References

1. Weinstein LS, Shenker A, Gejman PV, Merino MJ, Friedman E, Spiegel AM. Activating mutations of the stimulatory G protein in the McCune-Albright syndrome. N Engl J Med. 1991;325:1688–95.
2. Schwindinger WF, Francomano CA, Levine MA. Identification of a mutation in the gene encoding the alpha subunit of the stimulatory G protein of adenylyl cyclase in McCune-Albright syndrome. Proc Natl Acad Sci U S A. 1992;89:5152–6.
3. Riminucci M, Saggio I, Robey PG, Bianco P. Fibrous dysplasia as a stem cell disease. J Bone Miner Res. 2007;21(Suppl 2):P125–31.
4. Corsi A, Cherman N, Donaldson DL, Robey PG, Collins MT, Riminucci M. Neonatal McCune-Albright syndrome: a unique syndromic profile with an unfavorable outcome. JBMR Plus Forthcoming Epub. 2018. https://doi.org/10.1002/jbm4.10134.
5. Ippolito E, Bray EW, Corsi A, et al. Natural history and treatment of fibrous dysplasia of bone: a multicenter clinicopathologic study promoted by the European Pediatric Orthopaedic Society. J Pediatr Orthop B. 2003;12:155–77.
6. Riminucci M, Fisher LW, Shenker A, Spiegel AM, Bianco P, Gehron Robey P. Fibrous dysplasia of bone in the McCune-Albright syndrome: abnormalities in bone formation. Am J Pathol. 1997;151:1587–600.
7. Riminucci M, Liu B, Corsi A, et al. The histopathology of fibrous dysplasia of bone in patients with activating mutations of the Gs alpha gene: site-specific patterns and recurrent histological hallmarks. J Pathol. 1999;187:249–58.
8. Bianco P, Riminucci M, Majolagbe A, et al. Mutations of the GNAS1 gene, stromal cell dysfunction, and osteomalacic changes in non-McCune-Albright fibrous dysplasia of bone. J Bone Miner Res. 2000;15:120–8.
9. Corsi A, Collins MT, Riminucci M, et al. Osteomalacic and hyperparathyroid changes in fibrous dysplasia of bone: core biopsy studies and clinical correlations. J Bone Miner Res. 2003;18:1235–46.
10. Riminucci M, Kuznetsov SA, Cherman N, Corsi A, Bianco P, Gehron Robey P. Osteoclastogenesis in fibrous dysplasia of bone: in situ and in vitro analysis of IL-6 expression. Bone. 2003;33:434–42.
11. Plotkin H, Rauch F, Zeitlin L, Munns C, Travers R, Glorieux FH. Effect of pamidronate treatment in children with polyostotic fibrous dysplasia of bone. J Clin Endocrinol Metab. 2003;88:4569–75.
12. Boyce AM, Kelly MH, Brillante BA, et al. A randomized, double blind, placebo-controlled trial of alendronate treatment for fibrous dysplasia of bone. J Clin Endocrinol Metab. 2014;99:4133–40.
13. Corsi A, Ippolito E, Robey PG, Riminucci M, Boyde A. Bisphosphonate-induced zebra lines in fibrous dysplasia of bone: histo-radiographic correlation in a case of McCune-Albright syndrome. Skeletal Radiol. 2017;46:1435–9.
14. Majoor BC, Appelman-Dijkstra NM, Fiocco M, van de Sande MA, Dijkstra PS, Hamdy NA. Outcome of long-term bisphosphonate therapy in McCune-Albright syndrome and polyostotic fibrous dysplasia. J Bone Miner Res. 2017;32:264–76.
15. Florenzano P, Pan K, Brown SM, et al. Age-related changes and effects of bisphosphonates on bone turnover and disease progression in fibrous dysplasia of bone. J Bone Miner Res. 2019;34:653–60.
16. Yamamoto T, Ozono K, Kasayama S, et al. Increased IL-6-production by cells isolated from the fibrous bone dysplasia tissues in patients with McCune-Albright syndrome. J Clin Invest. 1996;98:30–5.
17. Stanton RP, Hobson GM, Montgomery BE, Moses PA, Smith-Kirwin SM, Funanage VL. Glucocorticoids decrease interleukin-6 levels and induce mineralization of cultured osteogenic cells from children with fibrous dysplasia. J Bone Miner Res. 1999;14:1104–14.
18. De Boysson H, Johnson A, Harlan N, Hajlaoui W, Auzary C, Geoffrey L. Tocilizumab in the treatment of a polyostotic variant of fibrous dysplasia of bone. Rheumatology (Oxford). 2015;54:1747–9.
19. Boyle WJ, Simonet WS, Lacey DL. Osteoclast differentiation and activation. Nature. 2003;423:337–42.
20. Wada T, Nakashima T, Hiroshi N, Penninger JM. RANKL-RANK signaling in osteoclastogenesis and bone disease. Trends Mol Med. 2006;12:17–25.
21. Piersanti S, Remoli C, Saggio I, et al. Transfer, analysis, and reversion of the fibrous dysplasia cellular phenotype in human skeletal progenitors. J Bone Miner Res. 2010;25:1103–16.
22. Zhao X, Deng P, Iglesias-Bartolome R, et al. Expression of an active Galphas mutant in skeletal stem cells is sufficient and necessary for fibrous dysplasia initiation and maintenance. Proc Natl Acad Sci U S A. 2018;115:E428–37.
23. Boyce AM, Chong WH, Yao J, et al. Denosumab treatment for fibrous dysplasia. J Bone Miner Res. 2012;27:1462–70.
24. Yamagishi T, Kawashima H, Ogose A, et al. Receptor-activator of nuclear kappaB ligand expression as a new therapeutic target in primary bone tumors. PLoS One. 2016;11:e0154680.
25. de Castro LF, Burke AB, Wang HD, et al. Activation of RANK/RANKL/-OPG pathway is involved in the pathophysiology of fibrous dysplasia and associated with disease burden. J Bone Miner Res. 2019;34:290–4.
26. Khan SK, Yadav PS, Elliott G, Hu DZ, Xu R, Yang Y. Induced Gnas(R201H) expression from the endogenous Gnas locus causes fibrous dysplasia by up-regulating Wnt/beta-catenin signaling. Proc Natl Acad Sci U S A. 2018;115:E418–27.
27. Ganda K, Seibel MJ. Rapid biochemical response to denosumab in fibrous dysplasia of bone: report of two cases. Osteoporos Int. 2014;25:777–82.
28. Benhamou J, Gensburger D, Chapurlat R. Transient improvement of severe pain from fibrous dysplasia of bone with denosumab treatment. Joint Bone Spine. 2014;81:549–50.

29. Eller-Vainicher C, Rossi DS, Guglielmi G, et al. Prompt clinical and biochemical response to denosumab in a young adult patient with craniofacial fibrous dysplasia. Clin Cases Miner Bone Metab. 2016;13: 253–6.
30. Saggio I, Remoli C, Spica E, et al. Constitutive expression of Gsalpha(R201C) in mice produces a heritable, direct replica of human fibrous dysplasia bone pathology and demonstrates its natural history. J Bone Miner Res. 2014;29:2357–68.
31. Kamijo S, Nakajima A, Ikeda K, et al. Amelioration of bone loss in collagen-induced arthritis by neutralizing anti-RANKL monoclonal antibody. Biochem Biophys Res Commun. 2006;347:124–32.
32. Body JJ, Facon T, Coleman RE, et al. A study of the biological receptor activator of nuclear factor-kappaB ligand inhibitor, denosumab, in patients with multiple myeloma or bone metastases from breast cancer. Clin Cancer Res. 2006;12:1221–8.
33. Henry DH, Costa L, Goldwasser F, et al. Randomized, double-blind study of denosumab versus zoledronic acid in the treatment of bone metastases in patients with advanced cancer (excluding breast and prostate cancer) or multiple myeloma. J Clin Oncol. 2011;29:1125–32.
34. Branstetter DG, Nelson SD, Manivel JC, et al. Denosumab induces tumor reduction and bone formation in patients with giant-cell tumor of bone. Clin Cancer Res. 2012;18:4415–24.
35. McClung MR, Lewiecki EM, Cohen SB, et al. Denosumab in postmenopausal women with low bone mineral density. N Engl J Med. 2006; 354:821–31.
36. Cummings SR, San Martin J, McClung MR, et al. Denosumab for prevention of fractures in postmenopausal women with osteoporosis. N Engl J Med. 2009;361:756–65.
37. Bone HG, Chapurlat R, Brandi ML, et al. The effect of three or six years of denosumab exposure in women with postmenopausal osteoporosis: results from the FREEDOM extension. J Clin Endocrinol Metab. 2013;98:4483–92.
38. Ominsky MS, Libanati C, Niu QT, et al. Sustained modeling-based bone formation during adulthood in cynomolgus monkeys may contribute to continuous BMD gains with denosumab. J Bone Miner Res. 2015;30:1280–9.
39. Negishi-Koga T, Shinohara M, Komatsu N, et al. Suppression of bone formation by osteoclastic expression of semaphorin 4D. Nat Med. 2011;17:1473–80.
40. Ikebuchi Y, Aoki S, Honma M, et al. Coupling of bone resorption and formation by RANKL reverse signalling. Nature. 2018;561: 195–200.
41. Ohishi M, Chiusaroli R, Ominsky M, et al. Osteoprotegerin abrogated cortical porosity and bone marrow fibrosis in a mouse model of constitutive activation of the PTH/PTHrP receptor. Am J Pathol. 2009;174: 2160–71.
42. Kuznetsov SA, Riminucci M, Ziran N, et al. The interplay of osteogenesis and hematopoiesis: expression of a constitutively active PTH/-PTHrP receptor in osteogenic cells perturbs the establishment of hematopoiesis in bone and of skeletal stem cells in the bone marrow. J Cell Biol. 2004;167:1113–22.
43. Ruffoni D, Fratzl P, Roschger P, Klaushofer K, Weinkamer R. The bone mineralization density distribution as a fingerprint of the mineralization process. Bone. 2007;40:1308–19.
44. Portal-Nunez S, Mediero A, Esbrit P, Sanchez-Pernaute O, Largo R, Herrero-Beaumont G. Unexpected bone formation produced by RANKL blockade. Trends Endocrinol Metab. 2017;28:695–704.
45. Nair AB, Jacob S. A simple practice guide for dose conversion between animals and human. J Basic Clin Pharm. 2016;7:27–31.
46. Dutta S, Sengupta P. Men and mice: relating their ages. Life Sci. 2016; 152:244–8.
47. Amgen I. Xgeva® (Denosumab) Prescribing Information [Internet]. Thousand Oaks, CA: Amgen, Inc.; 2013.